Quantitative analysis of third harmonic generation of XUV radiation in a cell and a cw free jet of carbon monoxide

F. Aguillon, A. Lebéhot, J. Rousseau, and R. Campargue

Citation: The Journal of Chemical Physics **86**, 5246 (1987); doi: 10.1063/1.452548
View online: http://dx.doi.org/10.1063/1.452548
View Table of Contents: http://scitation.aip.org/content/aip/journal/jcp/86/10?ver=pdfcov
Published by the AIP Publishing

Quantitative analysis of third harmonic generation of XUV radiation in a cell and a cw free jet of carbon monoxide

F. Aguillon, A. Lebéhot, J. Rousseau, and R. Campargue
Laboratoire des Jets Moléculaires, Département de Physico–Chimie, C. E. N. Saclay, 91191 Gif-sur-Yvette Cedex, France

(Received 12 November 1986; accepted 9 February 1987)

In the theory, the two-photon resonant third-order nonlinear susceptibility of a molecular gas is calculated. The variations of this susceptibility, with the rotational quantum numbers of the resonant states, are given in the case of two singlet states of different symmetries, Σ and Π. In the experiment, third harmonic generation of XUV light (94.5–97.5 nm) is obtained with and without two-photon resonance. The gaseous nonlinear medium is formed by CO as used either in a cell, or in a continuous supersonic free jet zone of silence. The intensity of the third harmonic wave generated is well related to the laser power, phase-matching conditions, two-photon resonances, and rotational temperature, through the nonlinear susceptibility, as described theoretically.

I. INTRODUCTION

In the past few years, the third harmonic generation (THG) and, more generally, the four-wave mixing techniques appeared to be very efficient for extending the current laser range to the VUV, and even the XUV regions. These wavelength domains are of great interest in chemical physics, in particular for going up to the ionized and Rydberg states of most molecules and atoms, and even to the first excited states of most light molecules and atoms.

Depending on the wavelength to be generated, different gases were used as nonlinear medium. Metallic vapors (Sr,[1,2] Mg,[3–6] Hg,[7–9] Zn[10]) are the best candidates for generating the wavelengths greater than 100 nm while rare gases (Xe,[11–13] Ar,[14–16] Kr,[17,18] Ne[19]) allow the wavelength range to be extended below 100 nm. Molecular nonlinear media are also used to generate VUV and XUV radiation (H_2,[20,21] NO,[22] I_2,[23] N_2,[24] CO.[21,24,25,26]

When the wavelength of the generated electromagnetic wave is below the LiF cutoff (108 nm), it is of course impossible to perform wave mixing in a cell; the exit window of the cell is generally replaced by a pinhole (in front of which the laser is focused) and differential pumping to allow the VUV light to propagate. Another way to provide a windowless system consists in using a pulsed free jet instead of a gas cell.[12,26,27] Finally, it is also possible to use, as nonlinear medium, the zone of silence[28] of a continuous free jet.[29,30]

The goal of this paper is to present a quantitative investigation on the efficiency of the THG in the XUV range, as performed through a cell and a cw free jet of a molecular gas (CO), used as nonlinear media. The various effects of the laser power, phase-matching, two-photon resonance, and repartition of the molecules on their different rotational states, are shown and discussed.

II. THEORY

The polarization p of a gaseous nonlinear medium, as induced by an electric field $\mathscr{E}$, can be expanded over the odd terms of $\mathscr{E}$,[31]

$$p = \epsilon_0\chi^{(1)}\mathscr{E} + \epsilon_0\chi^{(3)}\mathscr{E}\mathscr{E}\mathscr{E} + \cdots , \tag{1}$$

where $\chi^{(1)}$ and $\chi^{(3)}$ are the linear and nonlinear susceptibilities. In the presence of strong fields made available especially in focusing lasers, the cubic term $\chi^{(3)}\mathscr{E}\mathscr{E}\mathscr{E}$ becomes significant with its two components: one, at the laser frequency ω, responsible for the self-action of the laser beam; the other one, at the frequency 3ω, governing the THG.

The generated third harmonic power is given by[32–34]

$$P(3\omega) = \frac{27\omega^4}{4\pi^2\epsilon_0^2c^6}\frac{n^2(\omega)}{n^2(3\omega)}[N\chi^{(3)}(3\omega)]^2P^3(\omega)F(b\Delta k) , \tag{2}$$

where $P(\omega)$ is the laser power, b is the confocal parameter of the beam, N is the number density of the gaseous medium, and $n(\omega)$ and $n(3\omega)$ are the refractive indices for the laser and harmonic waves. The wave vector mismatch Δk is related to these indices by

$$\Delta k = \frac{3\omega}{c}[n(3\omega) - n(\omega)] . \tag{3}$$

The phase-matching factor $F(b\Delta k)$ reflects the interferences between the harmonic waves created at different points of the nonlinear medium. When the laser is focused at a distance f from the entrance window of an L length cell, this phase-matching factor is given by[32–34]

$$F(b\Delta k,L,d) = \left|\int_{(f-L)/b}^{L/b} \exp(-ib\Delta kx)\frac{2dx}{(1+ix)^2}\right|^2 \tag{4}$$

assuming a TEM_{00} mode for the laser. Figure 1 shows the variations of the phase matching factor F vs $b\Delta k$ for different geometrical conditions. It should be noted that the propagation of the harmonic wave is efficient only when Δk is negative. This is a very restrictive condition for the choice of the nonlinear medium, since Δk, as the dispersion, usually is positive.

The interaction between the electromagnetic field and a molecule is described by $\chi^{(3)}$. This nonlinear susceptibility is

 0021-9606/87/105246-11$02.10

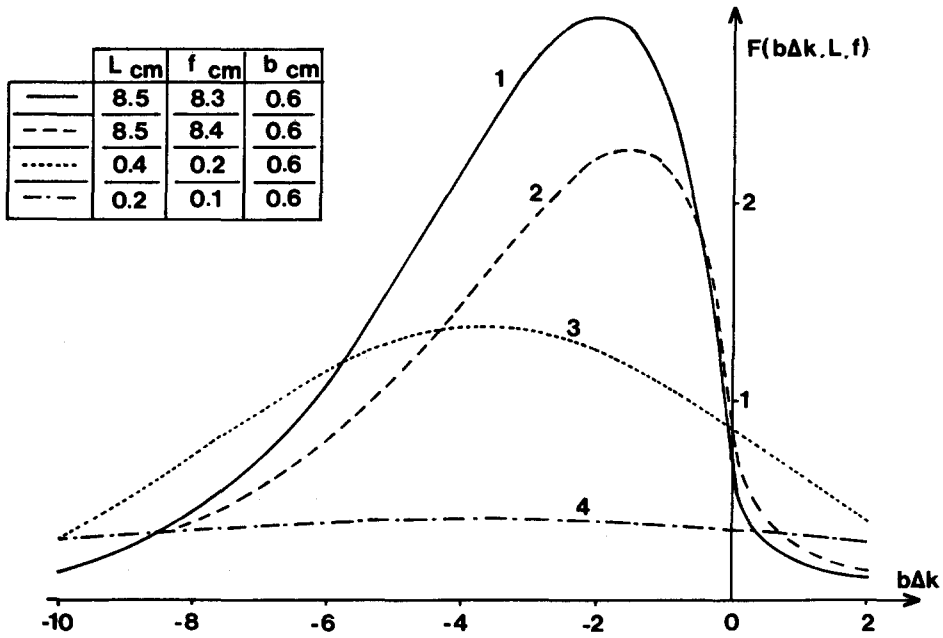

FIG. 1. Variations of the phase-matching factor vs $b\Delta k$. The curves 1 and 2 correspond to the typical geometry of a cell with the laser focused upstream and close to the exit orifice. The curves 3 and 4 correspond to the geometry used when focusing the laser near the nozzle throat of a free jet.

related to the induced polarization of the medium (1), which can be calculated using the density matrix ρ.

By introducing the relaxation phenomenologically, the equation of evolution can be written as[35]

$$\frac{d}{dt}\rho - i\hbar\Gamma(\rho^{(0)} - \rho) = [H^{(0)},\rho] - \mathscr{E}[\mu,\rho], \tag{5}$$

where Γ is the relaxation matrix, μ is the dipole moment operator, $\rho^{(0)}$ and $H^{(0)}$ are the density and Hamiltonian operators of the isolated molecule, and $\mathscr{E}$ is the electric field of the laser light.

The electric field $\mathscr{E}$, the polarization p, and the density matrix ρ can be expressed as Fourier series:

$$\mathscr{E} = \tfrac{1}{2}(\mathscr{E}_- e^{-i\omega t} + \mathscr{E}_+ e^{i\omega t}), \tag{6}$$

$$p = \sum_n \frac{1}{2}[p_-(n\omega)e^{-in\omega t} + p_+(n\omega)e^{in\omega t}], \tag{7}$$

$$\rho = \sum_n \frac{1}{2}[\rho_-(n\omega)e^{-in\omega t} + \rho_+(n\omega)e^{in\omega t}]. \tag{8}$$

The term driving the THG is[35]

$$N\chi^{(3)}(3\omega) = \frac{4Np_-(3\omega)}{\epsilon_0\mathscr{E}_-^3} = \frac{4N\,\mathrm{Tr}[\rho_-(3\omega)\mu]}{\epsilon_0\mathscr{E}_-^3}. \tag{9}$$

Equation (5) is expanded over the different orders of the perturbation and the various Fourier components $n\omega$. Since the frequency of $\mathscr{E}$ is ω and the frequency of the term of interest is 3ω [Eq. (9)], it is clear that the lowest order of perturbation needed is 3. In that way, Eq. (5) leads to

$$[\rho_-^{(n)}(n\omega)]_{ij} = \frac{\mathscr{E}_-}{2\hbar(\omega_{ij} - n\omega - i\Gamma_{ij})} \times [\mu,\rho_-^{(n-1)}(n\omega - \omega)]_{ij}. \tag{10}$$

The subscripts i and j refer to quantum states of the nonlinear medium.

It is of great interest to obtain this term for THG with two-photon resonance via an electronically excited state of the nonlinear medium. The two-photon resonance condition between a level of the ground state I and a level of an electronically excited state K can be written as $\omega_{KI} \approx 2\omega$. Due to the order of magnitude of ω (10^{16} Hz) and Γ (10^{11} Hz), the matrix $\rho_-^{(2)}(2\omega)$ can be reduced to its only component $[\rho_-^{(2)}(2\omega)]_{KI}$. Assuming that the K level is not populated, successive applications of Eq. (10) lead to

$$[\rho_-^{(2)}(2\omega)]_{KI} = \left(\frac{\mathscr{E}_-}{2\hbar}\right)^2 \frac{1}{\omega_{KI} - 2\omega - i\Gamma_{KI}} \frac{N(I)}{N} \times \sum_j \left(\frac{\mu_{Kj}\mu_{jI}}{\omega_{jI} - \omega}\right) \tag{11}$$

and then

$$N\chi^{(3)}(3\omega) = \frac{N(I)}{2\hbar^3\epsilon_0} \frac{1}{\omega_{KI} - 2\omega - i\Gamma_{KI}} \times \sum_{j,l} \left(\frac{\mu_{Il}\mu_{lK}\mu_{Kj}\mu_{jI}}{(\omega_{lI} - 3\omega)(\omega_{jI} - \omega)} - \frac{\mu_{Il}\mu_{lK}\mu_{Kj}\mu_{jI}}{(\omega_{Kl} - 3\omega)(\omega_{jI} - \omega)}\right). \tag{12}$$

At this point, it appears from Eqs. (2) and (12) that the third harmonic power depends only on the population of the resonant rotational level I. This is not surprising since the approximation used when reducing $\rho_-^{(2)}(2\omega)$ to $[\rho_-^{(2)}(2\omega)]_{KI}$ is equivalent to assuming that the contributions of all the rotational levels of the ground state other than level I, are negligible.

Now, it should be emphasized that the M degeneracy is not taken into account in Eq. (12). Nevertheless, because the laser polarization has to be linear (otherwise changes occurring in the M quantum number would lead to incoher-

ent processes), the different M sublevels remain separated. Each rotational level I splits into $2J_I + 1$ magnetic states I'; the population of each magnetic sublevel is $N(I') = [N(I)]/[2J_I + 1]$. Thus, Eq. (12) leads to

$$N\chi^{(3)}(3\omega) = \frac{N(I)}{2J_I+1}\frac{1}{2\hbar^3\epsilon_0}\frac{1}{\omega_{KI}-2\omega-i\Gamma_{KI}}\sum_{M=-J_I}^{+J_I}\sum_{jI'}\mu_{I'I}\mu_{I'K}\mu_{K'j}\mu_{jI'} \times\left[\frac{1}{(\omega_{II}-3\omega)(\omega_{jI}-\omega)}-\frac{1}{(\omega_{KI}-3\omega)(\omega_{jI}-\omega)}\right]. \tag{13}$$

Now the rotational line strength for THG can be derived from Eq. (13) by following very closely the calculation of Maïnos *et al.*[36] As far as the CO molecular levels involved in our experiment are singlet levels, the wave function of the molecule may be written as

$$|i\rangle = |\alpha_i\Lambda_i\rangle|J_i\Lambda_iM_i\rangle\,. \tag{14}$$

$|J_i\Lambda_iM_i\rangle$ is the rotational wave function in terms of the total angular momentum J_i, its projection Λ_i along the molecular axis, and its projection M_i along a laboratory axis. $|\alpha_i\Lambda_i\rangle$ is the vibronic wave function; α_i represents all quantum numbers except Λ_i. By transferring Eq. (14) into Eq. (13), it is obvious that the rotational line strength for resonant THG depends on

$$\mathscr{R} = \sum_M\sum_{jI}\langle\alpha_I\Lambda_I|\langle J_I\Lambda_IM|\mu|J_I\Lambda_IM\rangle|\alpha_I\Lambda_I\rangle\langle\alpha_I\Lambda_I|\langle J_I\Lambda_IM|\mu|J_K\Lambda_KM\rangle|\alpha_K\Lambda_K\rangle \times\langle\alpha_K\Lambda_K|\langle J_K\Lambda_KM|\mu|J_j\Lambda_jM\rangle|\alpha_j\Lambda_j\rangle\langle\alpha_j\Lambda_j|\langle J_j\Lambda_jM|\mu|J_I\Lambda_IM\rangle|\alpha_I\Lambda_I\rangle \times 1/[f^n(\omega,\omega_{II},\omega_{jI},\omega_{KI})]\,, \tag{15}$$

where the quantity $1/f^n(\omega,\omega_{II},\omega_{jI},\omega_{KI})$ appears between brackets in Eq. (13).

The wave functions may be written, in the case of a symmetric top, as[37,38]

$$|J\Lambda M\rangle = \left(\frac{2J+1}{8\pi^2}\right)^{1/2} D^{(J)}_{-M,-\Lambda}\,, \tag{16}$$

where $D^{(J)}_{-M,-\Lambda}$ is the Wigner matrix depending on the angles between the molecular and space, fixed frames. The dipole moment operator can be expressed, in the molecular fixed frame, for a linear polarization

$$\mu = \sum_{q=-1}^{1} D^{(1)*}_{0,q}\mu_q\,, \tag{17}$$

where the μ_q are defined in the molecular frame

$$\mu_0 = \mu_z\,,\quad \mu_{\pm1} = \frac{1}{\sqrt{2}}(\mu_x \pm i\mu_y)\,. \tag{18}$$

Now, transferring Eqs. (16) and (17) in Eq. (15), then neglecting the rotational contribution to the energy denominator, and finally using the closure relation over the intermediate j and l rotational wave functions, leads to

$$\mathscr{R} = \sum_M\sum_{jI}\sum_{q_1q_2q_3q_4}\frac{(2J_I+1)(2J_K+1)}{(8\pi^2)^2} \times\langle D^{(J_I)}_{-M,-\Lambda_I}|D^{(1)*}_{0q_1}D^{(1)*}_{0q_2}|D^{(J_K)}_{-M,-\Lambda_K}\rangle \times\langle D^{(J_K)}_{-M,-\Lambda_K}|D^{(1)*}_{0q_3}D^{(1)*}_{0q_4}|D^{(J_I)}_{-M,-\Lambda_I}\rangle \times\frac{\mu^{q_1}_{Ij}\mu^{q_2}_{jK}\mu^{q_3}_{Kl}\mu^{q_4}_{lI}}{f^n(\omega,\omega_{II},\omega_{jI},\omega_{KI})}, \tag{19}$$

μ^q_{ij} is defined by $\mu^q_{ij} = \langle\alpha_i\Lambda_i|\mu_q|\alpha_j\Lambda_j\rangle$.

In our experiment, the ground state belongs to the symmetry $^1\Sigma^+$ and the resonant state to the symmetry $^1\Pi$. Thus, $\Lambda_I = 0$ and $\Lambda_K = 1$, and the nonvanishing terms of the summation verify $q_1 + q_2 = -1$ and $q_3 + q_4 = 1$, with $q_{1234} = 0, \pm 1$. The only possibilities are $[(q_1 = 0$ and $q_2 = -1)$ or $(q_1 = -1$ and $q_2 = 0)]$ and $[(q_3 = 0$ and $q_4 = 1)$ or $(q_3 = 1$ and $q_4 = 0)]$. By using the formula contracting two Wigner matrices[37]

$$D^{(1)*}_{0,\pm1}D^{(1)*}_{0,0} = D^{(1)*}_{0,0}D^{(1)*}_{0,\pm1} = \frac{1}{\sqrt{3}}D^{(2)}_{0,\mp1}\,, \tag{20}$$

we obtain from Eq. (19),

$$\mathscr{R} = \sum_M\frac{(2J_I+1)(2J_K+1)}{3(8\pi^2)^2} \times|\langle D^{(J_I)}_{-M,0}|D^{(2)}_{0,1}||D^{(J_K)}_{-M,-1}\rangle|^2\mathscr{R}_{ev} \tag{21}$$

with

$$\mathscr{R}_{ev} = \sum_{jI}\sum_{q_1q_3}\frac{\mu^{q_1}_{Ij}\mu^{-1-q_1}_{jK}\mu^{q_3}_{Kl}\mu^{1-q_3}_{lI}}{f^n(\omega,\omega_{II},\omega_{jI},\omega_{KI})}. \tag{22}$$

The scalar product of three Wigner functions is given by[37,38]

$$\langle D^{(J)}_{MK}|D^{(J_1)}_{m_1k_1}|D^{(J_2)}_{m_2k_2}\rangle = 8\pi^2(-1)^{M+K}\begin{pmatrix}j_1 & j_2 & J\\ m_1 & m_2 & -M\end{pmatrix} \times\begin{pmatrix}j_1 & j_2 & J\\ k_1 & k_2 & -K\end{pmatrix}. \tag{23}$$

Thus,

$$\mathscr{R} = \frac{(2J_I+1)(2J_K+1)}{3}\left[\sum_M\begin{pmatrix}2 & J_K & J_I\\ 0 & -M & M\end{pmatrix}\right]^2 \times\begin{pmatrix}2 & J_K & J_I\\ 1 & -1 & 0\end{pmatrix}^2 \tag{24}$$

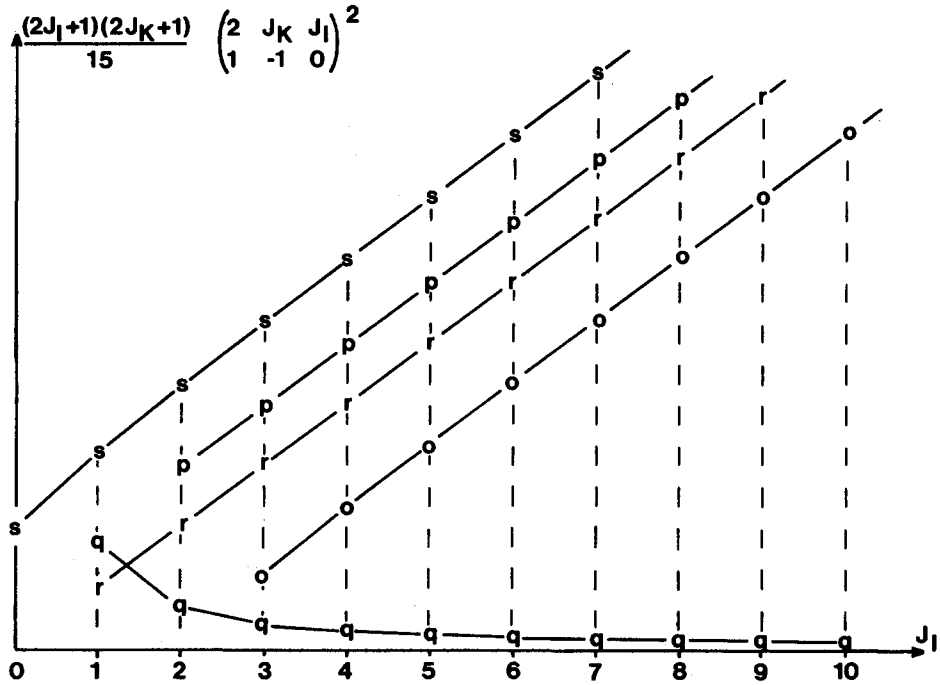

FIG. 2. Rotational dependence of the two-photon resonant third order nonlinear susceptibility. The five branches *O,P,Q,R,S*, allowed by the two-photon transition selection rules, correspond to $\Delta J = J_K - J_I = -2, -1, 0, 1, 2$. The particular behavior of the *Q* branch is corroborated by the absence of any observed resonant enhancement via two-photon *Q* transitions.

and this can be further simplified using the summation rule over the $3j$ coefficients[39]

$$\sum_M \begin{pmatrix}2 & J_K & J_I\\ 0 & -M & M\end{pmatrix}^2 = \frac{1}{5}. \tag{25}$$

Finally, the quantity $N\chi^{(3)}(3\omega)$ can be deduced from Eqs. (13), (24), and (25),

$$N\chi^{(3)}(3\omega) = \frac{N(I)}{2J_I+1}\frac{1}{2\hbar^3\epsilon_0}\frac{1}{\omega_{KI}-2\omega-i\Gamma_{KI}} \times \frac{(2J_I+1)(2J_K+1)}{15}\begin{pmatrix}2 & J_K & J_I\\ 1 & -1 & 0\end{pmatrix}^2 \mathscr{R}_{ev}. \tag{26}$$

The rotational dependence of the two-photon resonant nonlinear susceptibility is illustrated in Fig. 2. Although five branches are allowed by the two-photon selection rules, only the four branches *S*, *R*, *P*, *O* corresponding to $\Delta J = +2, +1, -1, -2$ are expected in the resonant THG spectra, brecause of the weakness of $\chi^{(3)}$ in the case of the *Q* branch.

The rotational line strength is essentially similar to the square of the two-photon absorption rotational line strength, as given in Refs. 40 and 41. This is consistent with the fact that the two-photon resonant THG can be regarded as two successive two-photon transitions ($I \rightarrow j \rightarrow K$ followed by $K \rightarrow l \rightarrow I$), as seen in Eq. (12).

III. EXPERIMENTAL SETUP

Figure 3 shows a scheme of the apparatus with the essential features. The laser system consists of a Nd:YAG pumped frequency doubled dye laser (Quantel model YG

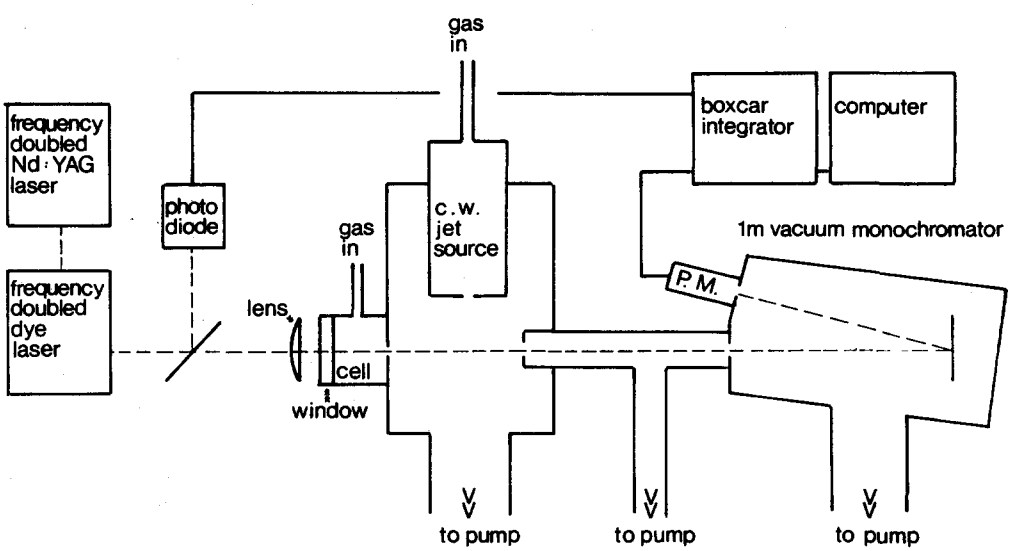

FIG. 3. Scheme of the experiment.

481, TDL IV). The laser beam is focused by a plano-convex lens ($f = 127$ mm) within the nonlinear medium. The laser power in the focus region ranges from 0.2 to 1.0 MW; the pulse duration is 10 ns, and the confocal parameter is $b = 6$ mm.

The nonlinear medium is a small volume of pure CO, located either in front of a 0.9 mm pinhole constituting the windowless exit of a cell, or on the centerline of the zone of silence[28] of a continuous supersonic free jet, as obtained from a stagnation pressure $P_0 = 2$ bars through a 220 μm diam nozzle. In both cases, differential pumping is used between the nonlinear medium and a 1 m vacuum monochromator (McPherson model 225), needed to separate the third harmonic wave from the laser light. The VUV signal is detected by an electron multiplier (Intertechnique model XP 1600), then treated by a boxcar integrator (Stanford Research System model 250), and finally recorded shot-per-shot by a microcomputer.

One of the main problems encountered in performing quantitative measurements of the frequency tripling concerns the laser stability. The difficulties arise from the dye laser crystal doubler, especially when scanning the wavelength. As a matter of fact, self-focusing of the UV light seems to occur in the KDP crystal together with the second harmonic generation. Thus, tuning the crystal phase-matching angle changes not only the laser power, but also the beam geometry. Moreover, the THG efficiency is found to be the most sensitive to geometrical variations when the KDP doubler is just phase matched. In order to get rid of this source of instabilities, the crystal is maintained in a position where the UV power is less than the maximum attainable power, but where the efficiency of the THG is almost insensitive to the variations of the phase-matching angle of the KDP crystal. This is performed by using as a feedback signal a small part of the UV light, in such a way that the efficiency of the second harmonic generation in the crystal doubler remains constant when scanning.

IV. COMPARISON OF THEORY WITH EXPERIMENT

A. Laser power dependence

As the detectors used are not fast enough with respect to the time of variation of the laser power, it is possible to measure only the power averaged over the duration of the laser pulse. Thus, the average value of $P(3\omega)$ has to be compared to the average value of $P^3(\omega)$, which depends not only on the measured average value of $P(\omega)$, but also on the temporal structure of $P(\omega)$ during the laser pulse. Thus, the fluctuations of the temporal structure of the laser pulse are accountable for the fluctuations in the conversion efficiency.

Figure 4 shows the dispersion of $P(3\omega)$, as attainable in a CO cell or free jet for a number of laser shots with the same power. This dispersion can be compared with the result of a computerized simulation of the same phenomenon. Because our laser presents a spectral width of 0.12 cm^{-1} for a cavity length of 50 cm, it can be modeled very simply by a laser delivering, with the same cavity, 12 longitudinal modes of equal amplitude and randomly varying phases. Figure 5 shows the dispersion of $P(3\omega)$ obtained with such a laser. The comparison of the simulated and experimental histograms (Figs. 4 and 5) shows rather good agreement. The discrepancies may be due to the fact that contrasted interferences, such as those given by the model due to the equality of the amplitudes for the different modes, improve the efficiency of the conversion. Moreover, it is assumed that each mode keeps the same phase during the pulse duration; phase jumps inside each mode would tend to smooth the dispersion curve.

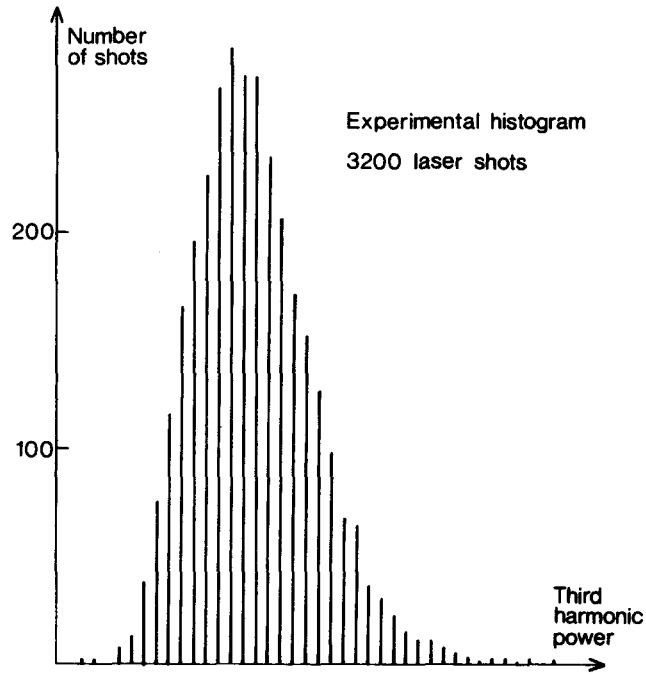

FIG. 4. Experimental distribution of the power of the third harmonic wave pulses, as recorded at constant laser power. The dispersion observed is due to the fluctuations of the laser pulse temporal structure.

By averaging a number of laser shots, one can illustrate the cubic dependence of $P(3\omega)$ on $P(\omega)$ as given by Eq. (2). Figure 6 shows the good agreement between theory and experiment, as usually obtained in the CO cell and free jet.

B. Phase matching

Unless the THG is obtained in a nonlinear medium much shorter than the confocal parameter b of the laser, the phase-matching factor (4) has significant values only if $b\Delta k$ is negative (Fig. 1). Thus, the frequency conversion is possible only if the nonlinear gaseous medium behaves with an abnormal dispersion for the generated wavelength. Due to the form of the dispersion curve in the vicinity of an absorption line, this condition is achieved on the blue side of the absorption domains. As an illustration of this effect, Fig. 7 shows the wavelength ranges where the THG has been observed in our laboratory, together with low-resolution absorption spectra of CO, as recorded using synchrotron radiation generated at the "Laboratoire pour l'Utilisation de Rayonnement Electromagnétique" (LURE) by the "Anneau de Collision d'Orsay" (ACO).[42] It is worth noting that this restrictive phase-matching condition is a good argument for using a molecular gas as nonlinear medium. As a matter of fact, the rare gases usually used below 100 nm are not able

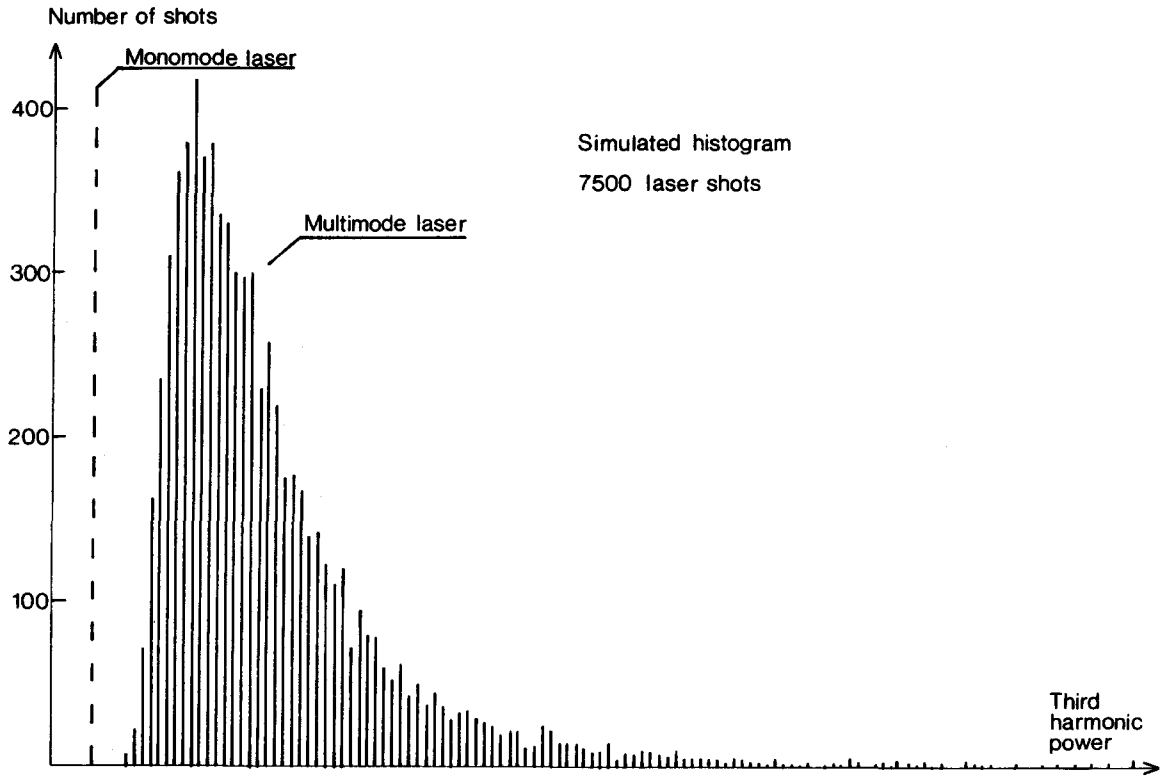

FIG. 5. Distribution of the power of the third harmonic wave pulses at constant laser power, as obtained by computerized simulation (see the text).

to cover continuously the XUV region; the molecules, with their very rich absorption spectra, make it possible to perform THG in a number of wavelength regions not attainable with rare gases.

The phase-matching factor is governed by the quantity $b\Delta k$, which varies as the gas pressure through the refractive indices of the medium (3). Thus, one can match the phase by changing the gas pressure. Equation (2) shows that the THG efficiency depends on $N, n(\omega)$, and $n(3\omega)$, also varying with the pressure. Nevertheless, as the nonlinear medium is gaseous, the variations of $n(\omega)/n(3\omega)$ can be neglected. Thus, as N is proportional to the pressure, and then to $b\Delta k$, the THG signal is expected to vary as $(b\Delta k)^2 F(b\Delta k)$. Figure 8 represents the variation of the third harmonic power with the pressure, together with theoretical curves computed for different distances between the laser focus and the exit hole of a cell containing carbon monoxide used as the nonlinear medium. Although the agreement seems to be very good for one of these curves, this may be due to the compensation of some errors. First of all, the theoretical

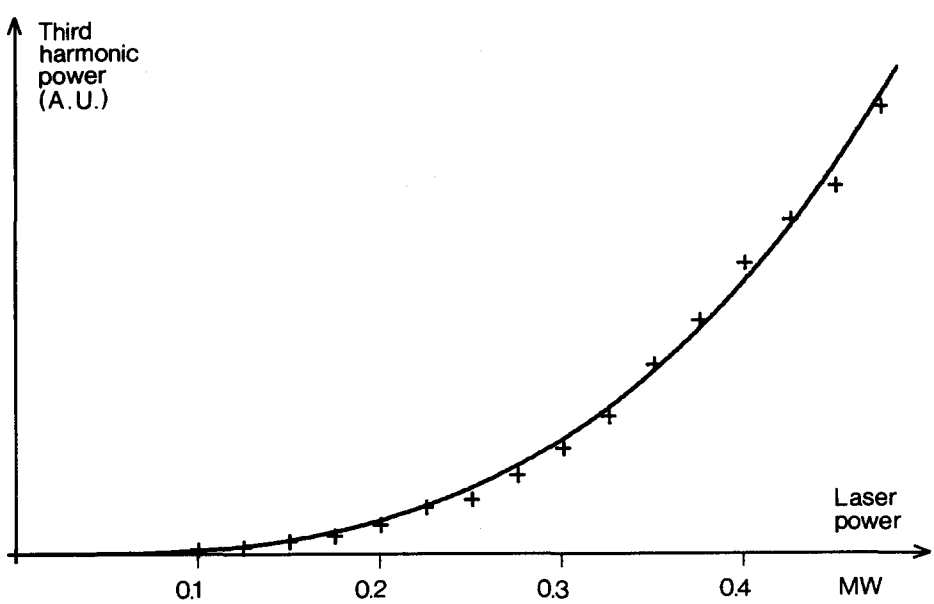

FIG. 6. Laser power dependence of the generated third harmonic power. The solid line is a cubic function of the laser power.

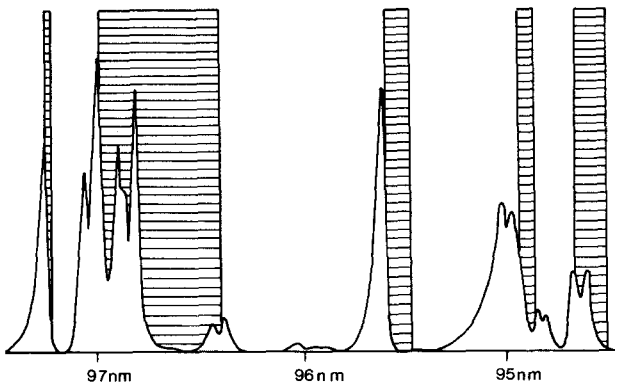

FIG. 7. Low resolution absorption spectrum of CO. The dashed zones represent the wavelength regions where significant THG has been observed in our laboratory. In these regions, the phase-matching condition can be fulfilled thanks to the abnormal dispersion occurring only on the blue side of the absorption bands.

curves assume that the gas pressure drops suddenly from its value within the cell to zero at the exit hole. This assumption may be not valid in our experiment where the laser focus to hole distance d is of the same order of magnitude as the size of the hole, which is a characteristic length of the pressure gradient. Moreover, since it is much stronger at high pressure than at low pressure, the self-absorption of the harmonic wave tends to distort the shape of the curve.

The THG can be performed in a number of wavelength regions (Fig. 7), with or without two-photon resonance. One of these nonresonant regions has been scanned for different pressures in the CO cell (Fig. 9). In this region, the phase matching is obtained thanks to the vicinity of a strong absorption band of CO around 95.63 nm.[42,43] It can be shown that the third harmonic power is governed by the phase-matching factor. From a qualitative point of view, the shape of the curves obtained when scanning the wavelength

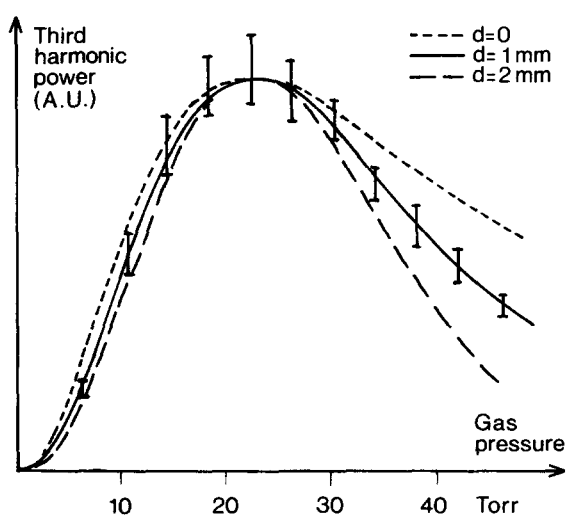

FIG. 8. Variations of the third harmonic power vs the pressure in the cell containing the gaseous nonlinear medium. The experimental points are compared to theoretical curves calculated for different distances d between the laser focus and the exit orifice of the cell.

can be explained by the fact that the wave vector mismatch Δk, on the blue side of an absorption band, increases continuously from very negative values near the absorption band, to a positive limit far from the absorption band. Thus, the quantity $b\Delta k$ governing the THG varies from highly negative values (leading to poor phase matching), to positive values (also leading to poor phase matching), through intermediate values giving good phase-matching conditions (Fig. 1). Moreover, since Δk varies as the pressure, the optimum value of Δk is reached for shorter wavelengths as the pressure increases, as shown in Fig. 9.

Due to the lack of data concerning the refractive indices in the VUV region, it is not possible to know the wave vector mismatch in this region. Nevertheless, a quantitative interpretation of Fig. 9 is possible with the assumption that the refractive index is constant at the laser wavelength and follows the Sellmeier relation for a single absorption line located at 95.63 nm in the XUV region. With these assumptions, the experimental curves can be fitted by the theoretical ones, using the phase-matching factor computed in the case of a focusing at 2 mm from the exit hole for the cell. The agreement means that the nonresonant THG is entirely governed by the phase-matching factor. The discrepancies observed on the red side of the curves may be due to the fact that the approximation used in considering that the absorption is due to a single line, instead of a band, becomes poorer as the wavelength increases; moreover, the computation assumes once again that the pressure suddenly drops to zero at the exit hole.

C. Resonant third harmonic generation

Two-photon resonant THG, involving the ground state $X\,^1\Sigma^+$, $v = 0$ and the levels $v = 1,2,3,4$ of the $A\,^1\Pi$ state of CO, has been detected; paths through other intermediate levels have not yet been explored. Depending on the vibrational level, the phase matching is more or less efficient, and rather good on the levels $v = 1$ and $v = 3$. Three-photon resonance has not been observed.

Figure 10 shows a THG spectrum recorded with two-photon resonance via the $v = 3$ band of the $A\,^1\Pi$ state. Two essential features have to be noted on these results. First, the phase matching is possible thanks to the existence of a strong absorption band at 96.89 nm (Fig. 7)[42,43]; the phase-matching factor is responsible for the shape of the envelope of the curve, as seen from the similarity of the curves of Fig. 9. Second, the strong structures are due to two-photon resonances with each peak assigned to a transition between two rotational states of the $X\,^1\Sigma^+$ and $A\,^1\Pi$ levels of CO. Such a two-photon transition gives rise to five branches in a band, corresponding to ΔJ ranging from -2 to $+2$. No peak is clearly assigned to a transition of the Q branch; this is not surprising because the calculation of the nonlinear third-order susceptibility leads to much weaker rotational line strength for the Q branch than for all four other branches (Fig. 2).

In resonant THG, only the resonant states of the nonlinear medium contribute significantly to the frequency conversion, as shown by transferring Eq. (26) in relation (2). Thus, only the number density of the resonant rotational

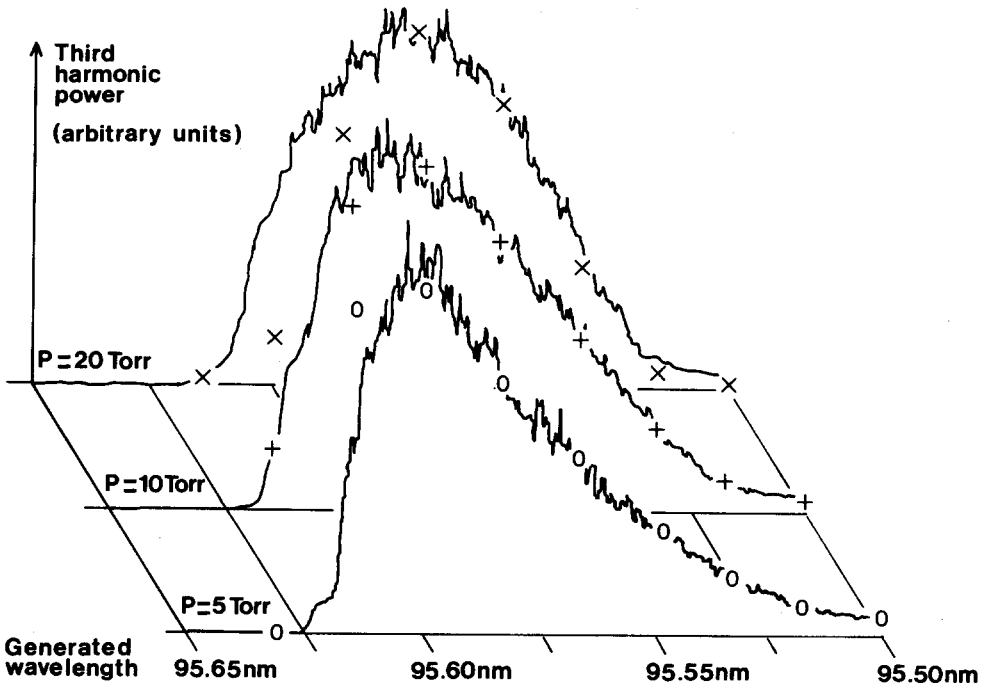

FIG. 9. Variations of the third harmonic power vs the wavelength recorded at three different pressures of the nonlinear gaseous medium contained in a cell. The points plotted close to and on the curves are the theoretical values obtained when assuming a Sellmeier-type variation of the refractive index.

state has to be taken into account, instead of the total number density of the gaseous medium, as in the nonresonant case. This has been observed directly by focusing the laser beam on the centerline of a supersonic free jet instead of a cell. Then, the rotational cooling due to the expansion of the gas leads to changes in the rotational population distribution and, consequently, in the relative intensities of the resonant THG lines corresponding to different J levels. This effect is clearly illustrated in Fig. 11. The amplitudes of the different spectra have been normalized to the $S(1)$ transition, since the decrease of the number density during the expansion is followed by a decrease of the THG efficiency. From Fig. 11, it is obvious that the low J levels are more and more populated as the gas expands in the jet. The particular behavior observed for $J = 0$ at low x/D is due to an overlap between the $S(0)$ and the $R(2)$, $R(3)$, and $R(4)$ two-photon transition lines. These R lines disappear with the flow cooling resulting from the expansion.

In order to make quantitative analysis on these population distribution effects, it is necessary to take into account

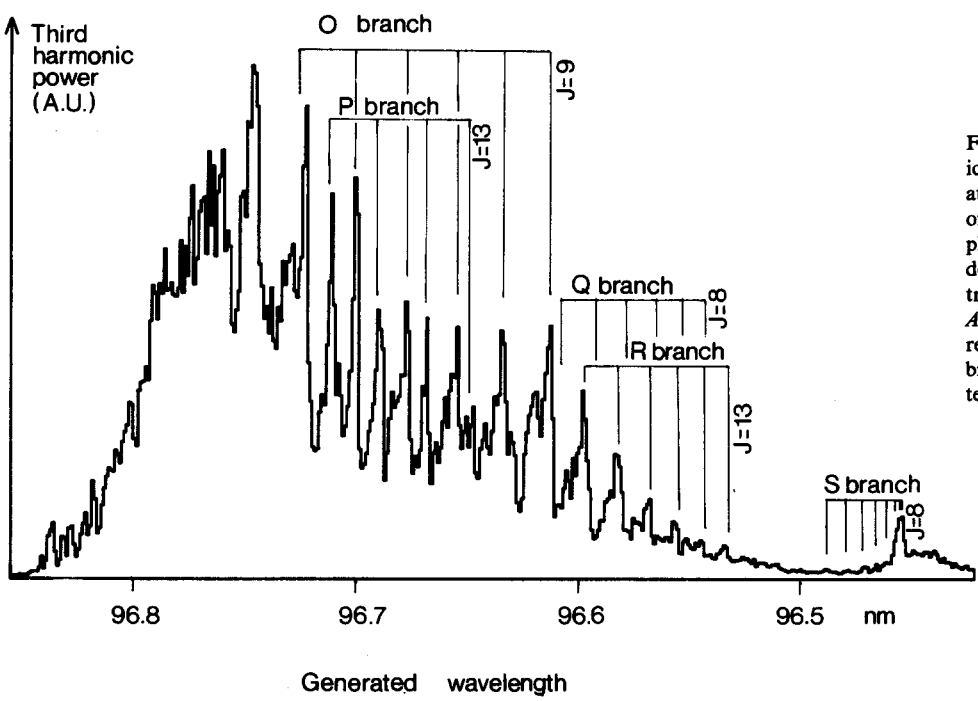

FIG. 10. Two-photon resonant third harmonic generation spectrum obtained in a CO cell, at a pressure $P = 10$ Torr. The general shape of the curve is due to the variation of the phase-matching factor along the wavelength domain scanned, while the structures are attributed to the two-photon resonances via the $A\,^1\Pi v = 3$ levels of CO. The assignment of the resonant lines reveals the absence of the Q branch, as expected from theory (see the text).

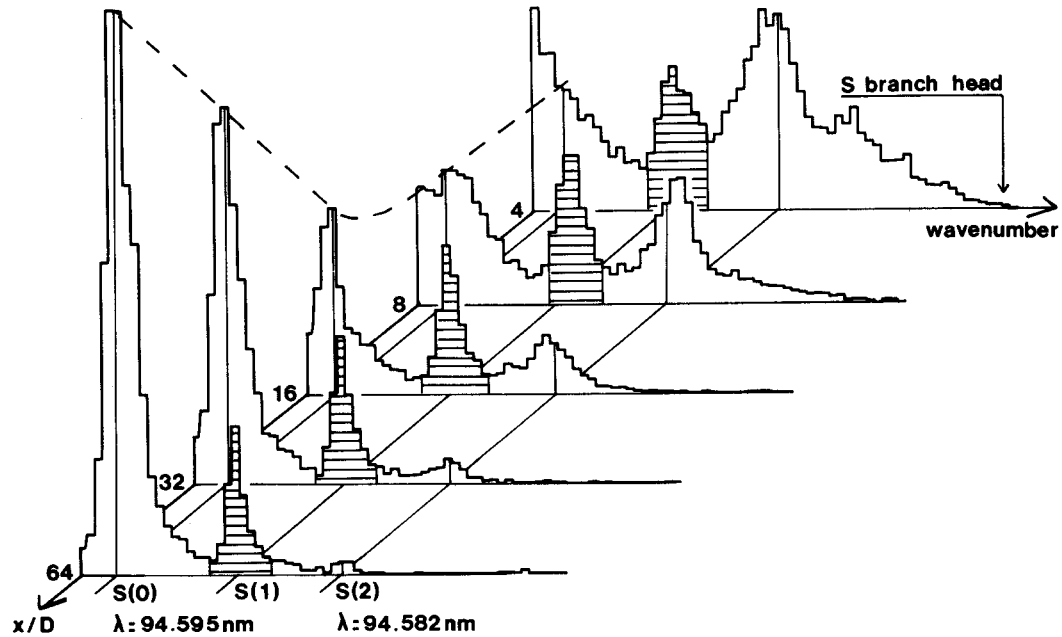

FIG. 11. Qualitative illustration of the rotational cooling occurring in a supersonic free jet. The five spectra of two-photon resonant THG via the $A\ ^1\Pi v = 4$ level of CO are recorded at different laser beam–nozzle throat distances x (in nozzle diameter D), and renormalized using the $S(1)$ transition. The dashed line shows the evolution of the $S(0)$ two-photon resonant THG signal with distance x. As the rotational temperature of the nonlinear medium decreases, the relative intensities of the low J resonant THG lines increase. The particular behavior observed at low x/D for $J = 0$ is explained in the text.

the variation of the phase-matching factor occurring when scanning the wavelength. As indicated above, it is not possible to know this phase-matching factor; the only possibilities consist in limiting the wavelength range scanned and choosing a region where the refractive indices are slowly varying. Moreover, in a free jet, there are two interesting possibilities for limiting the variations of the phase-matching factor. On one hand, the laser is focused near the nozzle throat, where the length of the nonlinear medium is smaller than the confocal parameter b; in these conditions, the phase-matching factor is a slowly varying function of $b\Delta k$ (Fig. 1). On the other hand, with increasing nozzle–laser distance, the rarefaction of the gas becomes so high that the wave vector mismatch, which varies as the density, can always be replaced by zero in the expression of the phase-matching factor; $\Delta k = 0$ is a poor condition for an efficient conversion, but a good condition for constant Δk. These two possibilities of maintaining nearly constant $b\Delta k$ by using a cw free jet as nonlinear medium, are of great interest in our quantitative analysis presented in this paper.

Due to the rotational cooling in the jet, the THG spectra are greatly simplified because the molecules are distributed only on a few rotational states. This makes much more realistic the approximation used in the calculation of the nonlinear susceptibility $\chi^{(3)}$, by neglecting the contribution of all nonresonant states with regard to that of the resonant states. Also, in the experiment, the enhancement obtained for the state number densities, increases significantly the fraction of molecules involved in resonant THG. Consequently, the detection of the generated power is very easy, even at the gas density low enough for having negligible variations, with wavelength, of the phase-matching factor. The pulsed jets have similar advantages, but they are not so well defined as the cw jets in terms of the flow properties and partition of the molecules to their internal states.

All these considerations lead us to choose the resonant THG involving the S branch of the two-photon resonance between the $X\ ^1\Sigma^+$, $v = 0$ and $A\ ^1\Pi$, $v = 2$ levels of CO expanding in a free jet, in order to perform quantitative measurements on the population distribution effects in resonant THG. An example of a spectrum obtained with scanning this S branch is presented in Fig. 12, together with a simulated

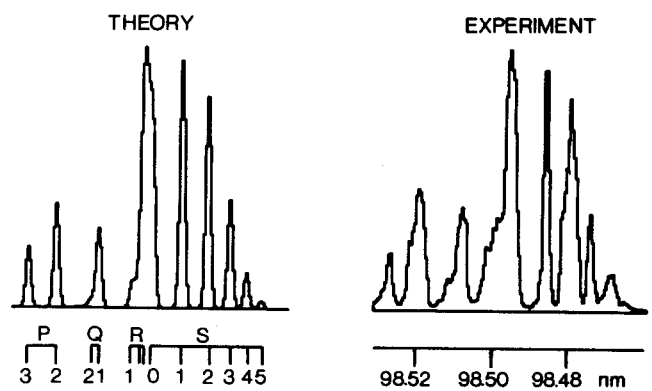

FIG. 12. Theoretical (left-hand side) and experimental (right-hand side) spectra of two-photon resonant THG via the $A\ ^1\Pi v = 2$ level of CO. The experimental spectrum has been recorded in a supersonic free jet. The theoretical spectrum has been calculated using a Boltzmann distribution and the rotational dependence of the nonlinear susceptibility, and assuming a constant wave vector mismatch throughout the wavelength domain scanned.

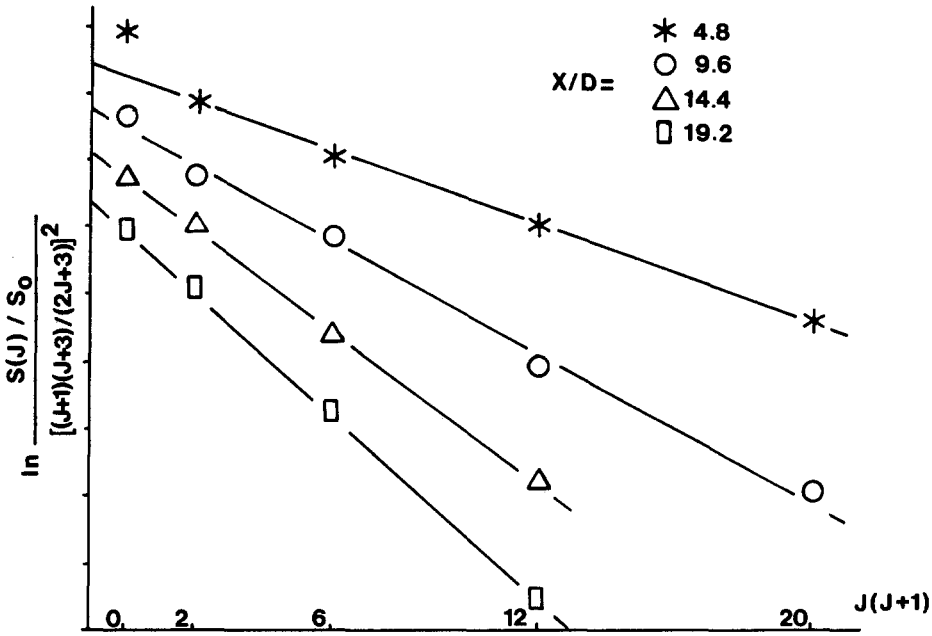

FIG. 13. Boltzmann plot obtained from two-photon resonant spectra involving the S branch of a two-photon transition between the levels $X\,^1\Sigma^+$, $v=0$ and $A\,^1\Pi$, $v=2$ of CO in a supersonic free jet, as recorded for different laser beam–nozzle throat distances x/D. The deviation from Boltzmann equilibrium, at low distance x/D, and low J, is only apparent (see the text).

spectrum computed assuming a Boltzmann distribution in the free jet. The only adjusted parameters in the simulation are the temperature and the linewidth. It should be emphasized that the phase-matching factor is, under the experimental conditions, quite constant all over a wavelength range wider than the S branch. In the case of an S branch, Eqs. (2) and (26) predict a VUV signal $S(J)$ originating from a J level such that $S(J)$ verifies

$$\ln \frac{S(J)}{[(J+1)(J+3)/(2J+3)]} = -\frac{2B}{kT} + \text{const}. \tag{27}$$

Figure 13 illustrates this relation for various nozzle–laser distances. The apparent deviation occurring for the $J=0$ line of the highest temperature is in fact due to the overlapping of the $S(0)$ line with the $R(3)$ and $R(4)$ lines, which are very close together (98.496 and 98.497 nm, respectively).[44] Finally, Fig. 14 shows a comparison of the rotational temperatures deduced from Fig. 13 and those computed assuming an isentropic expansion of the gas with $\gamma = 7/5$.[45,46]

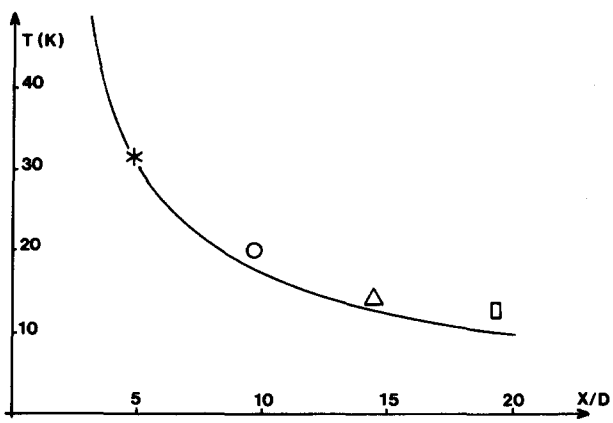

FIG. 14. Comparison between the temperatures deduced from Fig. 13 and those computed by assuming an isentropic expansion (solid line).

These results can be compared to those obtained by Rettner *et al.*[26] in similar experiments but using a pulsed jet instead of a continuous free jet. Their results are in qualitative agreement with ours, but they do not reflect a Boltzmann distribution. This could result from the higher laser power used in Stanford for obtaining the maximum conversion efficiency, apparently without taking care of the beam geometry stability; thus, deviations from equilibrium, as observed in our laboratory, can be due to phase-matching factor variations, saturation phenomena, and competing effects such as multiphoton ionization.

Wallace *et al.*[22] also obtained similar results by studying the intensities of the two-photon resonant THG lines. The THG was performed in a cell using nitric oxide as the nonlinear medium. They found a good agreement with the theoretical curves by scanning one resonance branch; for another branch, the agreement was not so good because of a fortuitous three-photon resonance enhancement, and probably phase-matching effects due to the vicinity of an absorption line and the harmonic wave generated.

V. CONCLUSION

This paper has presented new theoretical and experimental results on third harmonic generation in CO, in the XUV range. The calculation of the two-photon resonant nonlinear susceptibility can be generalized to any n-photon resonant nonlinear susceptibility. The experimental work has been performed with the greatest care to get rid of instabilities and with limited laser power to avoid saturation phenomena. Then, close agreement has been found between cell experiments and theory, with regard to the phase matching. Also, it has been shown that a cw free jet of the Campargue type,[28] as produced with a zone of silence surrounded by a shock wave structure, is a versatile gaseous nonlinear medi-

um for generating XUV radiation. In particular, these continuous free jets are much better defined than pulsed jets (as employed previously in Stanford,[26] apparently with mainly the goal of achieving maximum third harmonic radiation). Consequently, the knowledge of the properties of the cw free jets used as nonlinear media and also the simplification due to the very low rotational temperature obtained in these jets by adiabatic expansion, make it possible to check the validity of our theoretical calculation of the two-photon resonant third order susceptibility.

From a different point of view, now based on this calculation, resonant THG can be regarded as a new method to probe the state number densities in rarefied gaseous media. The main advantage of this method results from the fact that the signal is produced only in the laser focus region, and this is of great interest for spatial resolution. Moreover, the generated wave is able to propagate through the gas outside the focus region without significant wavelength dependent attenuation, even if the gaseous medium is not homogeneous. These two interesting advantages are not encountered in the usual probing techniques as those based on absorption, spontaneous, or laser-induced fluorescence spectroscopy.[46,47]

[1]R. T. Hodgson, P. P. Sorokin, and J. J. Wynne, Phys. Rev. Lett. **32**, 343 (1973).
[2]H. Schreinberger, H. Puell, and R. C. Vidal, Phys. Rev. A **18**, 2585 (1978).
[3]S. C. Wallace and G. Zdasiuk, Appl. Phys. Lett. **28**, 449 (1975).
[4]A. Timmermann and R. Wallenstein, Opt. Lett. **8**, 517 (1983).
[5]P. R. Herman, P. E. La Rocque, R. H. Lipson, W. Jamroz, and B. P. Stoicheff, Can. J. Phys. **63**, 1581 (1985).
[6]L. Zhao, Y. Nie, J. Zhang, Q. Li, and J. Yang, Opt. Commun. **58**, 281 (1986).
[7]P. R. Herman and B. P. Stoicheff, Opt. Lett. **10**, 502 (1985).
[8]R. Mahon and F. S. Tomkins, IEEE J. Quantum Electron. **QE-18**, 913 (1982).
[9]R. Hilbig and R. Wallenstein, IEEE J. Quantum Electron. **QE-19**, 1759 (1983).
[10]W. Jamroz, P. E. La Rocque, and B. P. Stoicheff, Opt. Lett. **7**, 617 (1982).
[11]H. Egger, R. T. Hawkins, J. Bokor, H. Pummer, M. Rotschild, and C. K. Rhodes, Opt. Lett. **5**, 282 (1980).
[12]A. H. Kung, Opt. Lett. **8**, 24 (1983).
[13]R. Hilbig and R. Wallenstein, IEEE J. Quantum Electron. **QE-19**, 194 (1983).
[14]J. Reintjes, Opt. Lett. **5**, 342 (1980).
[15]R. Hilbig and R. Wallenstein, Opt. Commun. **44**, 283 (1983).
[16]E. E. Marinero, C. T. Rettner, R. N. Zare, and A. H. Kung, Chem. Phys. Lett. **95**, 486 (1983).
[17]R. Mahon, T. J. MacIlrath, and D. W. Koopman, Appl. Phys. Lett. **33**, 305 (1978).
[18]R. Hilbig and R. Wallenstein, Opt. Appl. **21**, 913 (1982).
[19]R. Hilbig, A. Lago, and R. Wallenstein, Opt. Commun. **49**, 297 (1984).
[20]T. Srinivasan, H. Egger, H. Pummer, and C. K. Rhodes, IEEE J. Quantum Electron. **QE-19**, 1270 (1983).
[21]H. Pummer, T. Srinivasan, H. Egger, K. Boyer, T. S. Luk, and C. K. Rhodes, Opt. Lett. **7**, 93 (1982).
[22]S. C. Wallace and K. K. Innes, J. Chem. Phys. **72**, 4805 (1980).
[23]C. Tai and Y. Wu, Opt. Commun. **58**, 217 (1986).
[24]L. Hellner and J. Lukasik, Opt. Commun. **51**, 347 (1984).
[25]J. H. Glownia and R. K. Sander, Appl. Phys. Lett. **40**, 648 (1982).
[26]C. T. Rettner, E. E. Marinero, R. N. Zare, and A. H. Kung, J. Phys. Chem. **88**, 4459 (1984).
[27]J. Bokor, P. H. Bucksbaum, and R. R. Freeman, Opt. Lett. **8**, 217 (1983).
[28]R. Campargue, J. Phys. Chem. **88**, 4466 (1984).
[29]F. Aguillon, A. Lebéhot, J. Rousseau, and R. Campargue, *Proceedings of the 10th International Symposium on Molecular Beams* (Cannes, France, 1985), pp. VII, I, 1–3.
[30]F. Aguillon, A. Lebéhot, J. Rousseau, and R. Campargue, in *Rarefied Gas Dynamics*, edited by V. Boffi and C. Cercignani (Teubner, Stuttgart, 1986) Vol. II, p. 565.
[31]C. Flytzanis, *Quantum Electronics*, edited by Rabin and Tang (Academic, New York, 1975) Vol. I, Part A.
[32]J. F. Ward and G. H. C. New, Phys. Rev. **185**, 57 (1969).
[33]R. B. Miles and S. E. Harris, IEEE J. Quantum Electron. **QE-9**, 470 (1973).
[34]G. C. Bjorklund, IEEE J. Quantum Electron. **QE-11**, 287 (1975).
[35]J. F. Reintjes, *Nonlinear Optic Parametric Processes in Liquids and Gases* (Academic, Orlando, 1984).
[36]C. Maïnos, Y. Le Duff, and E. Boursey, Mol. Phys. **56**, 1165 (1985).
[37]A. R. Edmonds, *Angular Momentum in Quantum Mechanics* (Princeton University, Princeton, NJ, 1957).
[38]A. S. Davydov, *Quantum Mechanics* (NEO, Ann Arbor, 1967).
[39]L. Landau and E. Lifchitz, *Mécanique Quantique* (MIR, Moscow, 1967).
[40]R. G. Bray and R. M. Hochstrasser, Mol. Phys. **31**, 1199 (1976).
[41]J. B. Halpern, H. Zacharias, and R. Wallenstein, J. Mol. Spectrosc. **79**, 1 (1980).
[42]C. Letzelter (to be published).
[43]R. E. Huffman, J. C. Larrabee, and Y. Tanaka, J. Chem. Phys. **40**, 2261 (1964).
[44]S. G. Tilford and J. D. Simmons, J. Phys. Chem. Ref. Data **1**, 147 (1972).
[45]M. A. Gaveau, Thesis, University of Paris XI, Orsay, France, 1984.
[46]R. Campargue, M. A. Gaveau, and A. Lebéhot, in "*Rarefied Gas Dynamics*" edited by H. Oguchi (University of Tokyo, Tokyo, 1984), Vol. II, pp. 551–566.
[47]M. A. Gaveau, J. Rousseau, A. Lebéhot, and R. Campargue in *Gas Flow and Chemical Lasers*, edited by M. Onorato (Plenum, New York, 1984), pp. 483–490.